Widely accessible method for superresolution fluorescence imaging of living systems

Peter Dedecker[a,b,1], Gary C. H. Mo[a], Thomas Dertinger[c], and Jin Zhang[a,d,e,1]

[a]Department of Pharmacology and Molecular Sciences, [d]The Solomon H. Snyder Department of Neuroscience, and [e]Department of Oncology, The Johns Hopkins University School of Medicine, Baltimore, MD 21205; [b]Department of Chemistry, University of Leuven, Celestijnenlaan 200F, Heverlee, Belgium; and [c]SOFAST, 10999 Berlin, Germany

Edited* by Peter N. Devreotes, The Johns Hopkins University School of Medicine, Baltimore, MD, and approved May 22, 2012 (received for review March 22, 2012)

Superresolution fluorescence microscopy overcomes the diffraction resolution barrier and allows the molecular intricacies of life to be revealed with greatly enhanced detail. However, many current superresolution techniques still face limitations and their implementation is typically associated with a steep learning curve. Patterned illumination-based superresolution techniques [e.g., stimulated emission depletion (STED), reversible optically-linear fluorescence transitions (RESOLFT), and saturated structured illumination microscopy (SSIM)] require specialized equipment, whereas single-molecule–based approaches [e.g., stochastic optical reconstruction microscopy (STORM), photo-activation localization microscopy (PALM), and fluorescence-PALM (F-PALM)] involve repetitive single-molecule localization, which requires its own set of expertise and is also temporally demanding. Here we present a superresolution fluorescence imaging method, photochromic stochastic optical fluctuation imaging (pcSOFI). In this method, irradiating a reversibly photoswitching fluorescent protein at an appropriate wavelength produces robust single-molecule intensity fluctuations, from which a superresolution picture can be extracted by a statistical analysis of the fluctuations in each pixel as a function of time, as previously demonstrated in SOFI. This method, which uses off-the-shelf equipment, genetically encodable labels, and simple and rapid data acquisition, is capable of providing two- to three-fold-enhanced spatial resolution, significant background rejection, markedly improved contrast, and favorable temporal resolution in living cells. Furthermore, both 3D and multicolor imaging are readily achievable. Because of its ease of use and high performance, we anticipate that pcSOFI will prove an attractive approach for superresolution imaging.

subdiffraction-limit | two-color imaging | membrane rafts

Fluorescence imaging has become one of the major avenues for analyzing various molecular events underlying cellular processes. Even though many fluorophores can be used as molecular labels, direct observation at the molecular length scale is hampered by the diffraction of light. To provide a more detailed image of molecular events in cells, a number of techniques have been recently developed that bestow far-field fluorescence microscopy with fundamentally unlimited spatial resolution (1, 2). These techniques, either based on patterned illumination [such as stimulated emission depletion (STED) microscopy (3, 4), reversible optically linear fluorescence transitions (RESOLFT) microscopy (5), and saturated structured illumination microscopy (SSIM) (6)] or repeated single-molecule localization [such as photo-activation localization microscopy (PALM), stochastic optical reconstruction microscopy (STORM), fluorescence-PALM (F-PALM), ground-state depletion microscopy (GSDIM) microscopy (7–10)], are capable of improving spatial resolution by over an order of magnitude. However, these methods still face limitations. STED, RESOLFT, and SSIM microscopy require specialized equipment, and are less amenable to repeated imaging of genetically labeled samples. On the other hand, techniques based on single-molecule localization are temporally demanding and require high signal-to-noise ratios, which often limit the technique to total internal reflection (TIRF) excitation. These complications have hindered their application by many potential users, whereas repeated, fast, and 3D imaging remains challenging, especially in living systems.

A recent addition to this field is superresolution optical fluctuation imaging (SOFI), based on the statistical analysis of temporal fluorescence fluctuations. SOFI does not require specialized equipment and can produce subdiffraction images over a broad range of imaging conditions, including low signal-to-noise and high background (11, 12). In SOFI, a dataset of tens or hundreds of images is acquired at high speed, using fluorophores that can switch between a fluorescent and nonfluorescent state repeatedly. Due to the continuous cycling of the fluorophores between these states, the recorded images are highly dynamic, with no two images identical. A superresolution picture is then extracted from this dataset by recording the fluorescence fluctuations in each pixel as a function of time and calculating the cumulant of the resulting distribution (11). The exact resolution improvement depends on the order of the analysis; a factor of n improvement can be achieved with the calculation of the n^{th} order cumulant (13). In addition to robust spatial resolution improvements, SOFI allows improved contrast, background rejection, and favorable temporal resolution (12). Whereas SOFI can be performed on any sufficiently sensitive imaging system, including confocal systems, in practice it is most conveniently applied to wide-field imaging systems (using a 2D detector) due to the increased efficiency afforded by the parallel readout of multiple pixels.

The main advantages of SOFI are its technical simplicity, merely requiring repeated image acquisitions without modifications to the imaging process itself, and its robustness to nonideal imaging conditions. Even though higher order correlations can become susceptible to noise-induced distortions, an ~80-nm resolution (third order) and an ~60-nm resolution (fourth order) have been achieved (11). The ability to achieve a high resolution mainly depends on the characteristics of the fluorophores. The fluorophores must display fluctuations that are sufficiently slow to be resolvable compared with the acquisition time (tens of milliseconds in practice), but persistent to be observable over the full measurement duration. This has largely limited the technique to quantum dots (11) and organic fluorophores in a carefully controlled buffer (14), hindering its application in most biological settings.

Author contributions: P.D. and J.Z. designed research; P.D. and G.C.H.M. performed research; T.D. contributed new reagents/analytic tools; P.D., G.C.H.M., T.D., and J.Z. analyzed data; and P.D. and J.Z. wrote the paper.

The authors declare no conflict of interest.

*This Direct Submission article had a prearranged editor.

[1]To whom correspondence may be addressed. E-mail: peter.dedecker@hotmail.com or jzhang32@jhmi.edu.

This article contains supporting information online at www.pnas.org/lookup/suppl/doi:10.1073/pnas.1204917109/-/DCSupplemental.

We set out to develop a superresolution imaging method for the real-time visualization of living biosystems based on SOFI. We found that reversibly photochromic labels produce highly robust intensity fluctuations in living systems without the need for special sample preparation. The resulting data provide a two- to threefold enhanced spatial resolution, markedly improved contrast, and a temporal resolution of a few seconds in living cells using a commercial "off the shelf" imaging system. We find that the same concepts are readily extendable to two-color and 3D imaging.

Results

Reversibly Photochromic Labels Provide Robust Single-Molecule Fluctuations. Despite their differences, almost all subdiffraction-limit fluorescence imaging techniques benefit from or require the use of fluorophores that possess specific physicochemical properties beyond the mere emission of a fluorescence photon in response to an excitation photon (15, 16). To search for a genetically encodable fluorescent label for fluctuation imaging, we chose to initially focus on the reversible photoswitchable fluorescent protein Dronpa (17–20). Dronpa can exist in a fluorescent or nonfluorescent state; both of which are thermally stable on a timescale of hours. Excitation of Dronpa with blue-green light (e.g., 515 nm) induces bright fluorescence emission, but also causes its fluorescence to disappear in time, from where it can be recovered very efficiently when irradiated with weak UV light (e.g., 405 nm). The high contrast and reversibility of this reversible photoswitching have allowed Dronpa to be used in a number of superresolution experiments (21, 22).

Despite its positive characteristics, the reversible photoswitching of Dronpa can be a complication in some cases. As shown in Fig. 1*A*, Dronpa fluorescence does not disappear completely when irradiated at 488 nm, but instead reaches a plateau at a very low level, a phenomenon also observed by other researchers (18, 20, 23). Using sensitive equipment this low emissive state can be visualized directly, painting a surprisingly dynamic picture in which the continuous activation and deactivation of individual molecules is apparent (best appreciated by viewing Movie S1). We attribute these single-molecule fluctuations to an equilibration of the light-induced on and off switching. Although there does not appear to be significant absorption by the nonfluorescent state at wavelengths used for the excitation of the fluorescence (Fig. 1*B*), this observation can be explained by noting that the efficiency of the on switching is orders of magnitude higher than that of the off switching (17), which compensates for the weak absorption of the 488-nm light by the nonfluorescent state. Further support for this hypothesis comes from our observation that over 90% of the fluorescence of Dronpa can be recovered by irradiating at 457 nm, a wavelength just slightly shorter than 488 nm. However, these fluctuations also appear when exciting at 514 nm, suggesting that both a protonated and deprotonated form of the chromophore may be involved (18). The fluctuations remain observable over several minutes or more of continuous irradiation, which allows them to be captured over many frames (Movie S1).

These data showed that Dronpa delivers robust single-molecule intensity fluctuations that are observable over extended periods. We hypothesized that this behavior of Dronpa provides a necessary, sufficient, and convenient way to achieve the requirements inherent to SOFI imaging (Fig. 1*C*). At the same time it also effectively solves the problem of labeling density: because the equilibrium favors the nonfluorescent state when Dronpa is excited at 488 nm, fluctuations caused by the stochastic on switching of individual fluorophores can be readily detected. Additionally, for samples that are sparsely labeled, the equilibrium could be shifted to favor the fluorescent state by using a more blue-shifted excitation wavelength or concomitant UV excitation.

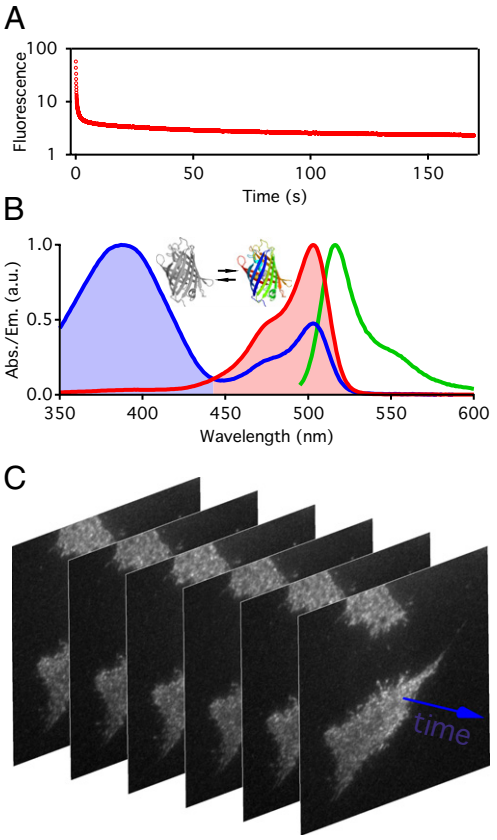

Fig. 1. Dronpa provides robust single-molecule fluctuations. (*A*) Detected fluorescence emission of a HeLa cell expressing Lyn-Dronpa upon irradiation at 488 nm. (*B*) Absorption spectra of Dronpa in the fluorescent (red) and nonfluorescent (blue) states and its emission spectrum excited at 488 nm (green). (*C*) Excerpt from a pcSOFI acquisition showing six consecutive images acquired on a HeLa cell expressing Lyn-Dronpa, revealing the subtle differences between the images due to the emitter fluctuations (see also Movie S1).

Superresolution Imaging. To determine whether this finding could lend itself to superresolution imaging, we fused Dronpa with a targeting motif derived from Lyn kinase, which targets the sphingolipid- and cholesterol-enriched microdomains within the plasma membrane (24). HeLa cells expressing Lyn-Dronpa were not treated in any way except to replace the medium with a balanced salt solution immediately before imaging on a TIRF microscope. Upon excitation with a 488-nm laser, we found that the initially bright fluorescence rapidly gave way to the dynamic fluctuations described above. We acquired 400–1,000 frames in rapid succession (10-ms exposure time per frame) and analyzed the resulting stack of images using a second-order cumulant analysis (11, 13) implemented in homemade software. As shown in Fig. 2, filopodia-like protrusions at the periphery and on the surface of the cell were highlighted in the processed image, similar to reported examples of fusion proteins targeted by the N-terminal sequence of Lyn kinase (24, 25). A comparison between the averaged raw image and the processed image showed a significant enhancement in resolution and contrast (Fig. 2). We quantified the increase in optical resolution (*SI Appendix*, *Supplementary Method*, and Fig. S1), and found an approximate factor-of-two improvement in spatial resolution (about 120 nm) compared with conventional image, consistent with our use of second-order cumulant analysis. This twofold-resolution increase can be obtained already from a low number of acquired images (*SI Appendix*, Fig. S2). We also found that some measurements,

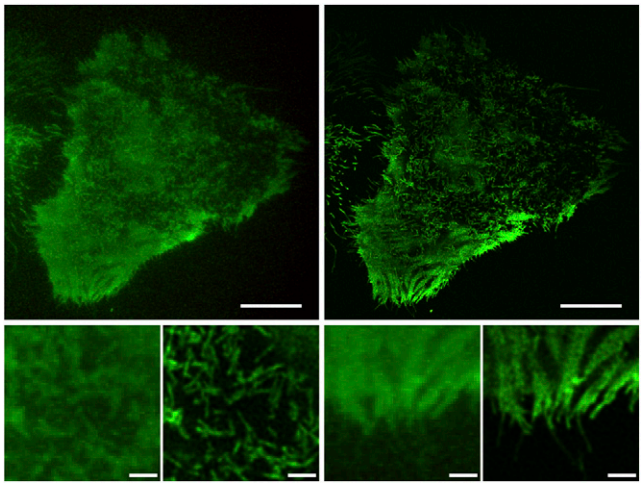

Fig. 2. Superresolution imaging with pcSOFI. Conventional (*Left*) and pcSOFI (*Right*) images acquired on a Lyn-Dronpa–labeled HeLa cell using TIRF-mode excitation. The smaller images show two expansions. (Scale bars, 10 μm in the main images and 1 μm in the expansions.)

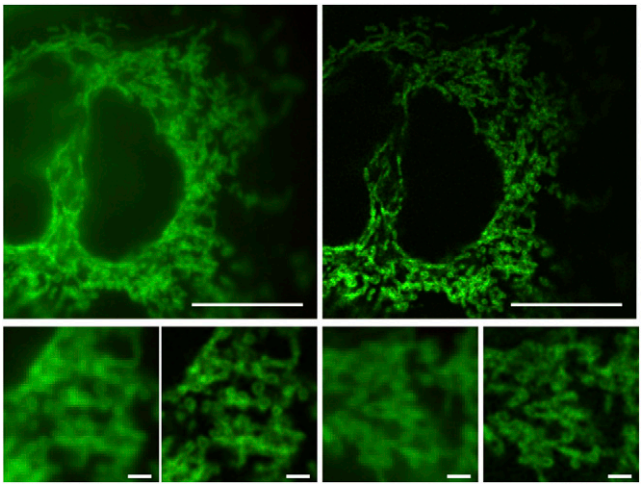

Fig. 4. pcSOFI in epifluorescence mode. Epi-mode section of a HeLa cell labeled with DAKAP-Dronpa visualized using conventional imaging (*Left*) and pcSOFI (*Right*). The smaller images show two expansions. (Scale bars, 10 μm in the main images and 1 μm in the expansions.)

especially those acquired using TIRF imaging, could be analyzed using a third-order cumulant and resulted in a further enhanced spatial resolution (Fig. 3 and *SI Appendix*, Figs. S3 and S4). Although this was not possible with all samples due to the increased sensitivity to noise, future optimization should help achieve this further enhancement of spatial resolution more readily. In addition to offering a higher imaging resolution, the pcSOFI images also contain twice or three times as many pixels compared with the raw image, which permits more detailed visualization of fine details. The additional pixels arise through the calculation of cross-cumulants between adjacent pixels (13).

Whereas TIRF imaging provides a high signal-to-noise ratio, it is limited to observing regions close to the surface. To test whether we could apply the pcSOFI strategy in the epifluorescence (epi) mode, we generated another construct containing Dronpa fused to a targeting sequence from DAKAP-1, which targets the outer membrane of mitochondria (26), and imaged HeLa cells expressing DAKAP-Dronpa using epi-illumination. The second-order processed image showed a significant enhancement in resolution and contrast (Fig. 4 and *SI Appendix*, Fig. S5). We observed slightly lower improvements (about 160 nm) for the DAKAP-targeted samples, which we attribute to a combination of reduced signal-to-noise and slight motion during the acquisition. Morphologies revealed by our DAKAP-targeted probe were in good agreement with previous imaging of the mitochondria (27), occasionally resolving hollow mitochondrial structures that were also seen in other superresolution imaging experiments (28). Thus, this method can be used on existing imaging systems in either TIRF or epi mode, providing a two- to threefold enhanced spatial resolution and a temporal resolution of a few seconds in living cells. The additional attributes include markedly improved contrast and enhanced background rejection (*SI Appendix*, Fig. S6). We termed this technique "photochromic stochastic optical fluctuation imaging" (pcSOFI).

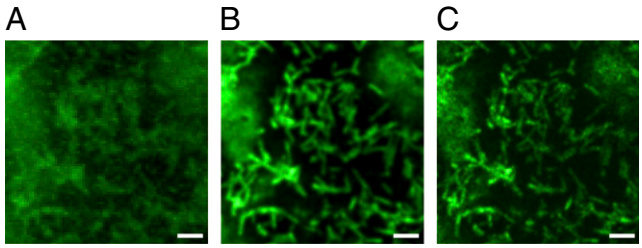

Fig. 3. Different analyses of pcSOFI. (*A*) conventional, (*B*) second-order, and third-order pcSOFI image showing an *Inset* of the measurement in Fig. 2. (Scale bars, 1 μm.)

Three Dimensional pcSOFI. Life is not restricted to two dimensions, and any comprehensive imaging technique should therefore adapt to fully 3D operation. Despite recent advances (29, 30), extended 3D imaging of live cells over a depth of several micrometers or more remains a challenge with most of the available superresolution imaging methods. This challenge is associated with the accelerated photodegradation that is typically a byproduct of the high intensities used in superresolution imaging, and the restriction to TIRF imaging due to the requirement of background reduction.

The robustness of the photochromism-based fluctuations in pcSOFI, as well as the inherent capacity of fluctuation imaging to deal with reduced signal-to-noise (12), led us to investigate *z*-stack–based 3D imaging. Using an excitation light of 488 nm, we performed a stack-based image acquisition on a living HeLa cell expressing DAKAP-Dronpa. Seven pcSOFI datasets were acquired in rapid succession, each spaced over a 0.5-μm interval and individually analyzed using the 2D cumulant. Each cumulant calculation considers only a single *xy* plane and effectively attenuates the contribution of out-of-focus fluorescence (11). A projection of the reconstructed 3D volume is shown in Fig. 5; the full set of projections is available as Movie S2. These data show the marked increase in detail that is available using pcSOFI. The total depth over which images could be acquired was mainly limited by the thickness of the cells. The imaging can be extended straightforwardly to thicker samples, with the caveat that success depends on a careful balance between imaging speed and chromophore photobleaching. Thus, 3D-pcSOFI provides a feasible way of producing 3D images of live cells at subdiffraction-limit resolution. Moreover, given the temporal resolution of a few seconds for each pcSOFI image, it also has the potential to reveal dynamic information in 3D.

Dual-Color pcSOFI. Multicolor imaging provides a powerful method for dissecting the dynamic interaction and compartmentalization of biomolecules. To achieve multicolor pcSOFI, we turned our

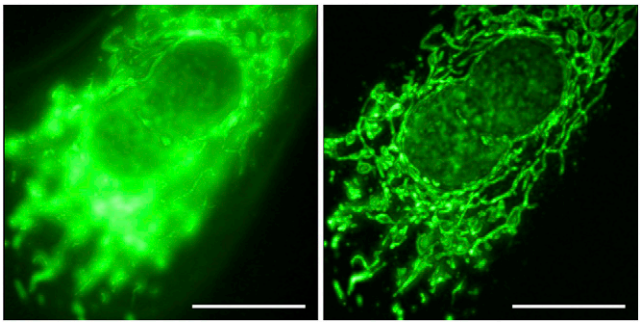

Fig. 5. 3D pcSOFI. Projection of a 3D stack recorded on a HeLa cell labeled with DAKAP-Dronpa. The full set of projections is available in Movie S2. *Left* and *Right* images denote the conventional and pcSOFI images, respectively. (Scale bar, 10 μm.)

attention to other switchable fluorescent proteins with a shifted spectrum compared with Dronpa. We considered the recently published rsTagRFP a candidate for pcSOFI due to its largely analogous photochromic behavior to Dronpa (31). We replaced Dronpa with rsTagRFP in the DAKAP and Lyn fusion constructs and imaged HeLa cells expressing Lyn-rsTagRFP and DAKAP-rsTagRFP. Analogous to what was observed with Dronpa, we found that illumination with a single wavelength of 561 nm led to significant fluctuations in rsTagRFP fluorescence (Movie S3 and *SI Appendix*, Figs. S7 and S8). Additionally, the spectral separation of Dronpa and rsTagRFP is sufficient to allow the distinguishing of their fluorescence (*SI Appendix*, Fig. S9).

For simultaneous two-color imaging, we prepared additional fusion constructs in which Dronpa and rsTagRFP are fused to a targeting motif derived from either K-ras4B or Lyn kinase. Kras targeting motif combines a farnesylated cysteine residue with a polybasic sequence to target nonraft microdomains in the plasma membrane (32). On the other hand, the targeting motif from Lyn kinase is known to target membrane raft microdomains through myristoylation and palmitoylation (24, 33, 34). We examined the localization of Lyn-rsTagRFP and Kras-Dronpa as well as Lyn-Dronpa and Kras-rsTagRFP using two-color pcSOFI. The dual-color imaging of Dronpa and rsTagRFP was performed in a sequential fashion, but can be interleaved to achieve approximate simultaneity. The necessity of sequential excitation in this case is due to the fact that the 488-nm irradiation required for Dronpa activates rsTagRFP, resulting in the disappearance of the fluctuations associated with the rsTagRFP photoswitching.

The results of the coimaging are summarized in Fig. 6. The distributions of the labels appear to be broadly similar in the conventional image, yet much more intricate and complex in the two-color pcSOFI image with resolution comparable to that achieved in single-color experiments (*SI Appendix*, Fig. S10). We quantified the apparent colocalization by calculating the thresholded Pearson's correlation coefficient, r, resulting in the data shown in Fig. 6*C*. The increased level of detail in the pcSOFI images results in a significant ($P < 10^{-4}$) decrease in correlation coefficient from 0.63 to 0.02. The lack of significant colocalization of Lyn-rsTagRFP and Kras-Dronpa is consistent with findings of a previous study in which a fluorescence resonance energy transfer (FRET) analysis showed fluorescent proteins targeted through myristoylation/palmitoylation and those through prenylation were not clustered (24). This is contrasted with control experiments where Dronpa and rsTagRFP were targeted to the same membrane raft domain (*SI Appendix*, Fig. S11). Furthermore, cell treatment with methyl-β-cyclodextrin (MβCD) to perturb membrane microdomains by partially depleting cholesterol resulted in a significant ($P < 10^{-4}$) increase in Dronpa/rsTagRFP colocalization in pcSOFI images (Fig. 6*C*). This result further supports the idea that membrane rafts and nonraft regions within the plasma membrane are functionally distinct and spatially segregated microdomains. These measurements demonstrate the direct applicability of pcSOFI in uncovering details that remain obscured in conventional imaging, while retaining the same level of convenience and ease of use.

Discussion

In this work we described a unique modality for superresolution imaging, pcSOFI, and show that it can be applied to yield fluorescence images with a subdiffraction limit spatial resolution. The key element in pcSOFI is the use of reversibly photochromic

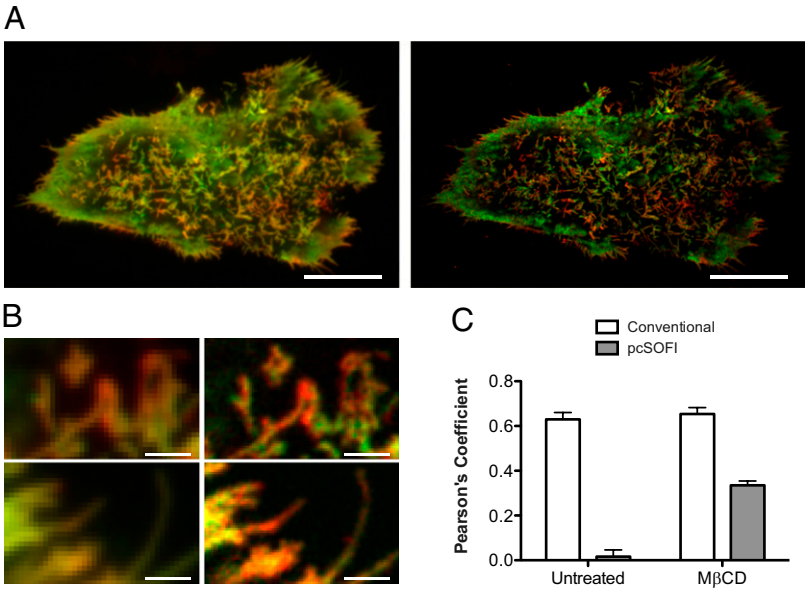

Fig. 6. Dual-color pcSOFI. (*A*) HeLa cell labeled with Lyn-Dronpa (green) and Kras-rsTagRFP (red), showing the conventional and pcSOFI image. (*B*) Expansions of areas in *A*. [Scale bars, 10 μm (*A*) and 1 μm (*B*), respectively.] (*C*) Bar chart showing the mean value of the thresholded Pearson's correlation coefficient calculated for the conventional and pcSOFI images with and without methyl-β-cyclodextrin (MβCD) treatment (error bars show the SEM, $n = 12$) ($P < 10^{-4}$).

labels, which generate robust single-molecule fluctuations when illuminated with light of an appropriate wavelength. We attribute this flickering to an equilibrium of the light-induced on and off switching. Furthermore, we expect that by tuning the excitation wavelength, the equilibrium distribution of fluorophore between the fluorescent and nonfluorescent state can be shifted. This adaptability, derived from the specific properties of the reversibly photoswitching fluorophores, could help cope with very different label concentrations in different samples, while allowing the imaging to be tailored to both fast acquisition and optimal performance.

Because the pcSOFI image is the result of a cumulant analysis, the computed intensities in each pixel of the image are no longer trivially related to the recorded fluorescence intensity (*SI Appendix*, *Supplementary Discussion*). However, the recorded signal is directly proportional to the local concentration provided that all fluorophores display the same switching and emission properties (11). Another issue that can complicate the quantitative analysis of pcSOFI images is the dependence of the image on the evenness of the illumination. However, this can be corrected straightforwardly by empirically measuring the evenness using a homogeneously fluorescent sample (e.g., a slide made of fluorescent plastic). In addition, pcSOFI imaging does not require that the fluorophores remain immobile throughout the measurement, and in general probe diffusion will not introduce artifacts except under certain conditions (*SI Appendix*, *Supplementary Discussion*).

The above implementation of pcSOFI represents a minimum learning curve for current users of conventional fluorescence imaging. This technique is compatible with a range of microscopy hardware operated in TIRF or epi mode, equipped with a sensitive camera (such as an electron-multiplying CCD) and using lasers or other light sources. Such systems are readily commercially available and are present in many research groups. The data acquisition is straightforward, and the postprocessing is done using software implemented in Igor Pro (called Localizer). By using genetically encoded labels, avoiding any special treatment or preparation, and using commonly used imaging systems, this technique should prove attractive to a large number of researchers.

In addition to being comparatively easy to implement, pcSOFI also shows strong performance. One attractive feature is the markedly reduced background and enhanced contrast in pcSOFI images. Cellular autofluorescence or other potentially interfering fluorophores that do not exhibit fast fluctuations on the acquisition time scale become essentially invisible in pcSOFI (*SI Appendix*, Fig. S6). Furthermore, unlike the point-scanning techniques such as STED and RESOLFT where imaging speed is influenced by the area of the image field and pixel size, or STORM/PALM/FPALM where temporal resolution is limited by the time required to accumulate sufficient fluorophore localization density, the temporal resolution of pcSOFI is determined by exposure time and number of frames required. In practical terms, this duration can be as short as 5 s under current conditions. Although dynamic processes occurring faster than this time scale could lead to blurring in our implementation, optimization of imaging conditions and available hardware as well as improved fluorescent labels should further improve the temporal resolution. Whereas the spatial resolution provided by pcSOFI is not as high compared with STED or PALM/STORM, it provides an attractive alternative for dynamic imaging of living systems with genetically encoded labels and offers convenience and compatibility with multicolor and 3D imaging. Perhaps the closest alternative to pcSOFI in terms of spatial resolution is structured illumination microscopy (SIM), and its nonlinear variant SSIM, both of which require extensive modifications to the imaging system. Compared with pcSOFI, SIM does not require special fluorophores, but is limited to a twofold increase in resolution. SSIM recently demonstrated a 40-nm resolution using the Dronpa photoswitching to induce fluorescence saturation (35), but requires a custom-built imaging system as well as the addition of a cytotoxic antifade reagent to counteract photodestruction of the label. Given its accessibility and strong performance, we expect that pcSOFI will ultimately prove to be a complementary and highly valuable addition to the existing superresolution techniques.

Materials and Methods

Constructs. Plasmids encoding Dronpa and rsTagRFP were kindly provided by Dr. Atsushi Miyawaki (RIKEN Brain Science Institute, Tokyo) and Dr. Vladislav Verkhusha (Albert Einstein College of Medicine, New York, NY). Dronpa and rsTagRFP were amplified by PCR and ligated into the pCDNA3 expression vector already containing the Lyn, Kras, or DAKAP targeting motifs.

Cell Transfection. HeLa cells were cultured in phenol red-free DMEM supplemented with 10% (vol/vol) FBS and plated onto sterilized glass coverslips mounted in 35-mm tissue culture dishes. Twenty-four hours before imaging these cells were transfected using either Lipofectamine 2000 (Invitrogen) according to the manufacturer's instructions or calcium phosphate-mediated transfection. We found that both approaches produced comparable results. Immediately before imaging, the cells were washed twice with HBSS and finally imaged in HBSS at ambient temperature.

Imaging. Imaging was performed on two different systems. The first system is a homebuilt TIRF system based on an Olympus IX-71 microscope equipped with a 100× NA 1.45 objective. Also installed on this setup is a Spectra-Physics 2018-RM multiline argon-krypton laser and a PhotoMetrics Cascade 512B electron-multiplied camera. This system was used to acquire the data in Figs. 2, 3, 4, and 5 and Movies S1 and S2, using 488 nm light from the laser in either epi or TIRF mode. Excitation and emission light were filtered using an Olympus C52009 filter cube. The total magnification of the imaging system resulted in an optical pixel size of about 109 nm.

The second system is an integrated and manufacturer-installed TIRF system from Nikon, based on a Ti-E inverted microscope and equipped with a 70-mW air-cooled argon ion laser and a 100-mW Coherent Sapphire 561-nm laser. Imaging was performed using a NA 1.49 CFI APO 100× TIRF objective and a manufacturer-installed GFP/RFP dual band dichroic. Emission was filtered using the included GFP and RFP filters, model numbers 89002 and 89017, respectively. Fluorescence was detected using a PhotoMetrics Evolve 512 × 512 electron-multiplied camera, with an optical pixel size of about 107 nm. This system was used to acquire the two-color data in Fig. 6 and Movie S3.

pcSOFI images were calculated from acquisitions containing between 400 and 3,000 frames, using either 488-nm excitation (Dronpa) or 561-nm excitation (rsTagRFP). We found little benefit from acquiring more than 1,000 frames. We found that EMCCD exposure times of 10–50 ms yielded satisfactory results, with the electron multiplication gain set to 3500 (Cascade) and 741 (Evolve). In general the optimal exposure time will depend on the excitation intensity, with higher excitation intensities allowing shorter acquisition times. In our hands we found that total excitation powers, measured after the objective in epi mode, of 3–7 mW were appropriate. Usable data could be acquired over acquisition times ranging from as low as 5 s to minutes. Whereas these excitation intensities may appear on the high side, we note that they are lower than or similar to the intensities typically used in PALM/STORM experiments. In fact, this imaging does not even require a laser light source: we have been able to acquire subdiffraction images with Dronpa using only the 100-W HBO lamp installed on the Olympus system.

Analysis. The acquired data were analyzed using the Localizer software developed for Igor Pro (WaveMetrics) and Matlab (MathWorks) involving a second-order cross-correlation based on previously published algorithms (11, 13). In addition to providing an increased spatial resolution, this calculation also provides an increased number of pixels through the calculation of cross-cumulants (13). Instead of the direct Fourier reweighing scheme published previously, which is fairly sensitive to measurement noise, we applied between two and six iterations of a Richardson-Lucy deconvolution (as implemented in Igor Pro) to obtain the full resolution increase afforded by the fluctuation imaging. For comparison, a conventional image was constructed by straightforward averaging of the frames used in the pcSOFI calculation. For reconstructing 3D projections we imported the calculated pcSOFI images into ImageJ (http://imagej.nih.gov/ij/) and made use of the built-in "3D project" functionality with the default settings. However, to render the increase

in detail clearly visible in the 3D projections, we artificially increased the spacing between the layers from the true value of 0.5 to 2 μm.

Colocalization analysis of the two-color data was based on the calculation of Pearson's correlation coefficient after image segmentation. Briefly, both the conventional and pcSOFI images were independently segmented using iterative thresholding as implemented in Igor Pro. The segmentation was applied to both the red and green channels, and these respective segmentations were combined using a logical OR operation to arrive at the applied segmentation. The correlation coefficient was then calculated using the "StatsCorrelation" operation in Igor Pro, including only nonbackground pixels as determined by the segmentation. We found that this analysis yielded essentially identical results using per-wavelength acquisition times ranging from 5 to 50 s. Of the 18 cells included in the analysis, 10 were transfected with Lyn-Dronpa and Kras- rsTagRFP, and the remaining 8 were transfected with Lyn-rsTagRFP and Kras-Dronpa, leading to very similar results. We checked the registration shift between the green and red emission channels by imaging TetraSpeck beads of 100 nm diameter (Molecular Probes) and recording the emission in both the green and red channels. The resulting registration shift was ~10 nm, which is negligible compared with the optical pixel size of the camera (107 nm).

ACKNOWLEDGMENTS. We thank Dr. Katie Herbst Robinson, Dr. Sohum Mehta, Dr. Vedangi Sample, and Mr. Wim Vandenberg for help in preparing some of the constructs and samples; Dr. Scot Kuo and The Johns Hopkins University School of Medicine Institute for Basic Biomedical Sciences microscope facility for technical assistance; and Dr. Philip Cole and Mr. Qiang Ni for critical reading of the manuscript. P.D. thanks the Research-Foundation Flanders (FWO-Vlaanderen) for a postdoctoral fellowship and travel grant. This work was supported by National Institutes of Health (NIH) Director's Pioneer Award DP1 OD006419 and NIH Grant R01 DK073368 (to J.Z.).

1. Hell SW (2007) Far-field optical nanoscopy. *Science* 316:1153–1158.
2. Huang B, Bates M, Zhuang X (2009) Super-resolution fluorescence microscopy. *Annu Rev Biochem* 78:993–1016.
3. Hell SW, Wichmann J (1994) Breaking the diffraction resolution limit by stimulated emission: Stimulated-emission-depletion fluorescence microscopy. *Opt Lett* 19: 780–782.
4. Klar TA, Jakobs S, Dyba M, Egner A, Hell SW (2000) Fluorescence microscopy with diffraction resolution barrier broken by stimulated emission. *Proc Natl Acad Sci USA* 97:8206–8210.
5. Hofmann M, Eggeling C, Jakobs S, Hell SW (2005) Breaking the diffraction barrier in fluorescence microscopy at low light intensities by using reversibly photoswitchable proteins. *Proc Natl Acad Sci USA* 102:17565–17569.
6. Gustafsson MG (2005) Nonlinear structured-illumination microscopy: Wide-field fluorescence imaging with theoretically unlimited resolution. *Proc Natl Acad Sci USA* 102:13081–13086.
7. Betzig E, et al. (2006) Imaging intracellular fluorescent proteins at nanometer resolution. *Science* 313:1642–1645.
8. Rust MJ, Bates M, Zhuang X (2006) Sub-diffraction-limit imaging by stochastic optical reconstruction microscopy (STORM). *Nat Methods* 3:793–795.
9. Hess ST, Girirajan TP, Mason MD (2006) Ultra-high resolution imaging by fluorescence photoactivation localization microscopy. *Biophys J* 91:4258–4272.
10. Fölling J, et al. (2008) Fluorescence nanoscopy by ground-state depletion and single-molecule return. *Nat Methods* 5:943–945.
11. Dertinger T, Colyer R, Iyer G, Weiss S, Enderlein J (2009) Fast, background-free, 3D super-resolution optical fluctuation imaging (SOFI). *Proc Natl Acad Sci USA* 106: 22287–22292.
12. Geissbuehler S, Dellagiacoma C, Lasser T (2011) Comparison between SOFI and STORM. *Biomed Opt Express* 2:408–420.
13. Dertinger T, Colyer R, Vogel R, Enderlein J, Weiss S (2010) Achieving increased resolution and more pixels with Superresolution Optical Fluctuation Imaging (SOFI). *Opt Express* 18:18875–18885.
14. Dertinger T, Heilemann M, Vogel R, Sauer M, Weiss S (2010) Superresolution optical fluctuation imaging with organic dyes. *Angew Chem Int Ed Engl* 49:9441–9443.
15. Manley S, et al. (2008) High-density mapping of single-molecule trajectories with photoactivated localization microscopy. *Nat Methods* 5:155–157.
16. Grotjohann T, et al. (2011) Diffraction-unlimited all-optical imaging and writing with a photochromic GFP. *Nature* 478:204–208.
17. Ando R, Mizuno H, Miyawaki A (2004) Regulated fast nucleocytoplasmic shuttling observed by reversible protein highlighting. *Science* 306:1370–1373.
18. Habuchi S, et al. (2005) Reversible single-molecule photoswitching in the GFP-like fluorescent protein Dronpa. *Proc Natl Acad Sci USA* 102:9511–9516.
19. Mizuno H, et al. (2008) Light-dependent regulation of structural flexibility in a photochromic fluorescent protein. *Proc Natl Acad Sci USA* 105:9227–9232.
20. Dedecker P, et al. (2006) Fast and reversible photoswitching of the fluorescent protein dronpa as evidenced by fluorescence correlation spectroscopy. *Biophys J* 91:L45–L47.
21. Dedecker P, et al. (2007) Subdiffraction imaging through the selective donut-mode depletion of thermally stable photoswitchable fluorophores: Numerical analysis and application to the fluorescent protein Dronpa. *J Am Chem Soc* 129:16132–16141.
22. Shroff H, et al. (2007) Dual-color superresolution imaging of genetically expressed probes within individual adhesion complexes. *Proc Natl Acad Sci USA* 104: 20308–20313.
23. Ando R, Flors C, Mizuno H, Hofkens J, Miyawaki A (2007) Highlighted generation of fluorescence signals using simultaneous two-color irradiation on Dronpa mutants. *Biophys J* 92:L97–L99.
24. Zacharias DA, Violin JD, Newton AC, Tsien RY (2002) Partitioning of lipid-modified monomeric GFPs into membrane microdomains of live cells. *Science* 296:913–916.
25. Lu S, et al. (2008) The spatiotemporal pattern of Src activation at lipid rafts revealed by diffusion-corrected FRET imaging. *PLOS Comput Biol* 4:e1000127.
26. Ma Y, Taylor S (2002) A 15-residue bifunctional element in D-AKAP1 is required for both endoplasmic reticulum and mitochondrial targeting. *J Biol Chem* 277: 27328–27336.
27. Safiulina D, Veksler V, Zharkovsky A, Kaasik A (2006) Loss of mitochondrial membrane potential is associated with increase in mitochondrial volume: Physiological role in neurones. *J Cell Physiol* 206:347–353.
28. Huang B, Jones SA, Brandenburg B, Zhuang X (2008) Whole-cell 3D STORM reveals interactions between cellular structures with nanometer-scale resolution. *Nat Methods* 5:1047–1052.
29. Shao L, Kner P, Rego EH, Gustafsson MG (2011) Super-resolution 3D microscopy of live whole cells using structured illumination. *Nat Methods* 8:1044–1046.
30. Jones SA, Shim SH, He J, Zhuang X (2011) Fast, three-dimensional super-resolution imaging of live cells. *Nat Methods* 8:499–508.
31. Subach FV, et al. (2010) Red fluorescent protein with reversibly photoswitchable absorbance for photochromic FRET. *Chem Biol* 17:745–755.
32. Roy MO, Leventis R, Silvius JR (2000) Mutational and biochemical analysis of plasma membrane targeting mediated by the farnesylated, polybasic carboxy terminus of K-ras4B. *Biochemistry* 39:8298–8307.
33. Gao X, Zhang J (2008) Spatiotemporal analysis of differential Akt regulation in plasma membrane microdomains. *Mol Biol Cell* 19:4366–4373.
34. Gao X, et al. (2011) PI3K/Akt signaling requires spatial compartmentalization in plasma membrane microdomains. *Proc Natl Acad Sci USA* 108:14509–14514.
35. Rego EH, et al. (2012) Nonlinear structured-illumination microscopy with a photoswitchable protein reveals cellular structures at 50-nm resolution. *Proc Natl Acad Sci USA* 109:E135–E143.